Two-Dimensional Incompressible Navier-Stokes Solver

Samir S. Kadri
Department of Mechanical and Industrial Engineering, University of Toronto

Abstract

This study developed and validated a steady, incompressible 2D Navier–Stokes solver for the lid-driven cavity benchmark using a finite-volume discretization on a uniform, collocated grid. Pressure–velocity coupling was handled through SIMPLE, with Rhie–Chow momentum interpolation used to compute face fluxes and prevent pressure checkerboarding. The resulting sparse systems were solved using GMRES with an AMG preconditioner, and convergence was assessed using a global continuity residual. The code allows the user to choose between the standard cavity (problem 1) and a stepped cavity (problem 2), where the step is treated as an internal no-slip wall. Centerline velocities and flow structures showed satisfactory agreement with Ghia et al. and a COMSOL Multiphysics simulation, while a mesh study across grids confirmed improved near-wall resolution with refinement.

Keywords: Incompressible Navier–Stokes; Lid-driven cavity; Finite-volume method; SIMPLE; Rhie–Chow interpolation.

Introduction

The steady, incompressible Navier-Stokes equations are the core CFD baseline, as they capture the essential physics for a wide range of flows while continuing to be simple enough that many high-quality references exist. One of which is the Lid Driven Cavity study, which is accepted as the benchmark test case for a newly developed CFD solver. Since the Lid-Driven Cavity is a tried and tested problem, validation material exists throughout the history of the field, much of which is used as the base of this paper.

Eq. (1) & Eq. (2) define the governing equations that represent the steady, incompressible momentum equation written in the vector form. Along with these equations, the study also assumes that the fluid properties are constant and exhibit Newtonian principles. Prior works on solvers aimed at tackling advection/diffusion cases were built upon to solve for the "Lid-Driven Cavity (LDC)" and the "LDC with step" problems for these governing equations.

A finite volume discretization was used, as shown in Appendix (1), along with a SIMPLE[1] framework and the Rhie-Chow interpolation[2] method for face fluxes on a collocated grid. Appendix (1) shows an in depth breakdown of the physics from a mathematical perspective and is the backbone of how the solver functions. An object-oriented Python solver was developed based on the discretization described, and the linear system of matrices assembled ($Ax = b$) was solved using the GMRES method combined with an AMG preconditioner.

To validate the results of the solver, the velocity field obtained was compared to Ghia *et al.*[3] and a COMSOL test case developed by the author, both with the same domain and mesh size as that being run using the developed code. Finally, a mesh convergence study was conducted, as shown in Appendix (2), to ensure that the mesh size being tested and validated was fine enough and non-erroneous.

$$\nabla \cdot \vec{u}\vec{u} = \nabla \cdot \nu \nabla \vec{u} - \frac{1}{\rho}\nabla p \tag{1}$$

$$\nabla \cdot \vec{u} = 0 \tag{2}$$

Problem Statement

The study aims to solve two problems: firstly, the classical lid-driven cavity problem, as shown in Fig. (1), after which further developments would be needed for the solution of the same lid-driven cavity, but with a step in one of the bottom corners, as shown in Fig. (2).

Both domains are of size 1×1, however the step is of size $1/3 \times 1/3$ and positioned in the bottom left. The lid is moving at 1 m/s and all boundary walls have the "no-slip condition." The Reynolds Number of the fluid is 100 in the simple LDC setup and 200 in the setup with the step. Both problems are solved for five grids; of mesh sizes around 33×33, 65×65, 129×129, 257×257, and 320×320. Finally, the program was tested on higher Reynolds numbers ($Re = 400$ & $Re = 1000$) to assess capabilities.

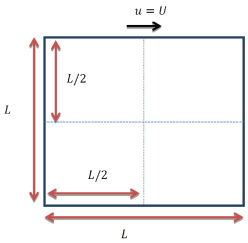

Figure 1: Problem setup for Lid Driven Cavity

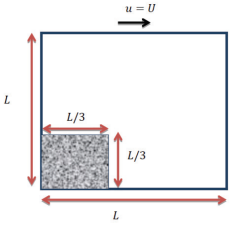

Figure 2: Problem setup for Lid Driven Cavity with step

Solution Methodology

A steady, two-dimensional incompressible Navier–Stokes solver was implemented in Python using a collocated finite-volume formulation on a uniform Cartesian grid. The domain of size $L_x \times L_y$ was discretized into a mesh with $N_x \times N_y$ control volumes with constant spacing, $\Delta x = L_x \div N_X$ & $\Delta y = L_y \div N_y$. Values of u, v & P were stored at cell centers with a layer of ghost cells on boundary. The lid-driven cavity boundary conditions were enforced as no-slip on the left, right, and bottom walls, i.e $u = v = 0$, while the "lid," or top wall, was given $u = 1$ & $v = 0$ to impose the moving lid condition.

Pressure boundary conditions were enforced using a zero-normal-gradient assumption by copying interior pressure values into the ghost cells, and a single reference pressure correction cell was pinned to remove the Neumann null space. The governing momentum equations were discretized using a finite-volume approach on a uniform, collocated grid, where diffusion was treated using central differencing and convection was handled using an upwind-stabilized formulation. This produced sparse linear systems for u & v, with under-relaxation applied through the modified diagonal coefficients and explicit source terms.

A SIMPLE framework was then used to handle pressure-velocity coupling: provisional velocities were obtained from the momentum solves, a pressure-correction equation was assembled from the continuity constraint, and u, v & P were updated using the correction. Since the solver is collocated, Rhie–Chow interpolation was used to compute face fluxes and prevent pressure checkerboarding.

The code was also made capable of allowing the user to choose between the two domains, the first one being the simple lid-driven cavity and the second being the LDC with a step, both of which are shown in Fig. (1) & Fig. (2) respectively. In problem 2, the step is treated as a solid through a fluid-mask approach, such that the step behaves as an internal no-slip wall. To do this, the face values of the wall adjacent cells were exactly zero, and the pressure values did not use central differences to avoid the influence of solid cell pressures. Finally, all assembled sparse systems were solved using GMRES with an AMG preconditioner, and convergence was assessed using a global continuity residual until the specified tolerance was met.

Results & Discussion

Each grid size run was set to converge at 10^{-6} to ensure results are accurate and comparable between each other. All the grid sizes showed a steady decay of the residual for around 1000 iterations at the coarsest grid ($N_x = N_y = 33$) to about 10,000 iterations at the finest grid ($N_x = N_y = 320$).

Solver solution time was very heavily dependent GMRES linear solver tolerances and AMG preconditioner rebuild intervals, as well as SIMPLE under-relaxation factors used. The tighter the GMRES tolerance, the more accurate the result per iteration tends to be; however, solution time increases with the same. On the other hand, with lower GMRES tolerances, time required for each iteration may decrease, but an overall increase in number of outer iterations was observed. Hence, the tolerances used for problem 1 were 10^{-8} for all, u, v & P, and 10^{-6}, 10^{-6} & 10^{-7} for u, v & P respectively in problem 2.

Under-relaxation factors also have a similar influence on the solver; at lower values, the convergence tends to be more robust but comes at the expense of a higher number of outer iterations, while higher values tend to increase convergence progress per iteration, but can lead to oscillations or even divergence in the residuals. For problem 1, under-relaxation factors were 0.6 for momentum and 0.4 for pressure, while they were set at 0.7 for momentum and 0.4 for pressure in problem 2.

Problem 1: Standard Lid-Driven Cavity

Fig. (3) and Fig. (4) show the velocity magnitude and pressure contours, while Fig. (5) shows velocity magnitude streamlines for the 257×257 grid. It is evident that the primary vortex occupies most of the cavity, while smaller corner vortices exist at the bottom two corners. It can also be observed that there is a high velocity gradient at the top, near the moving wall, producing thin shear layers.

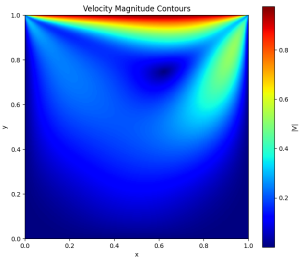

Figure 3: Contour of velocity magnitude for 257×257 grid, Re=100

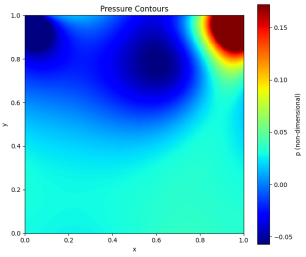

Figure 4: Contour of pressure for 257×257 grid, Re=100

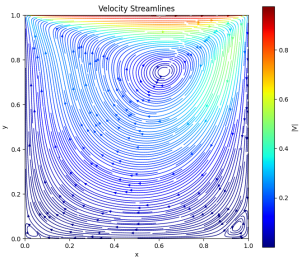

Figure 5: streamlines of velocity magnitude for 257×257 grid, Re=100

Fig. (6) shows the same domain being solved using COMSOL Multiphysics 6.3 as a source of validation. The centerline velocities were recorded from the 129×129 grid results of the program, as well as those from the COMSOL simulation, and plotted along with data from Ghia *et al.* in Fig. (7) and Fig. (8). The overlaid plots show satisfactory agreement and hence validate the accuracy of the results from the program.

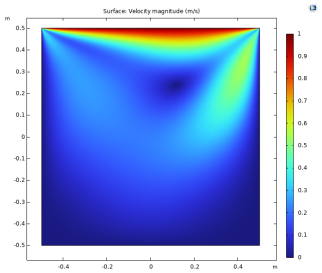

Figure 6: COMSOL validation: Contour of velocity magnitude for 257×257 grid, Re=100

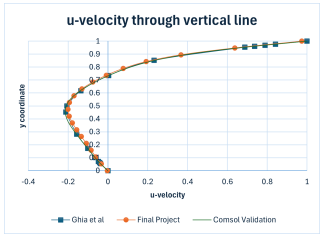

Figure 7: u-velocity through x=0.5

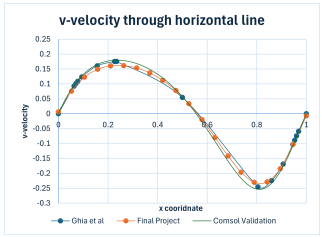

Figure 8: v-velocity through y=0.5

A mesh convergence was also performed, as shown in Appendix (2). Overall, the solver reproduces the standard LDC structure and matches the reference centerline profiles closely, with mesh refinement improving near-wall accuracy.

To ensure the program is capable of solving for higher Reynolds numbers, the same domain was tested on a 257×257 grid with $Re = 400$ & $Re = 1000$, streamline plots of which are shown in Fig. (9), and Fig. (10) respectively. It can be observed from these plots that as the Reynolds Number increases, the size of the smaller vortices increases significantly. This observation is consistent with the results provided in Ghia *et al.* and can be explained by the reduced viscosity of the fluid which leads to weaker viscous damping, allowing vorticity to persist and be advected into the corners more effectively, thereby strengthening and enlarging the secondary recirculation zones.

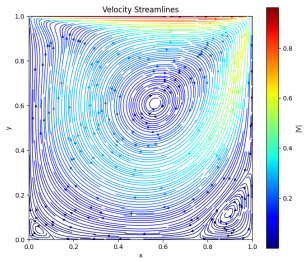

Figure 9: streamlines of velocity magnitude for 257×257 grid, Re=400

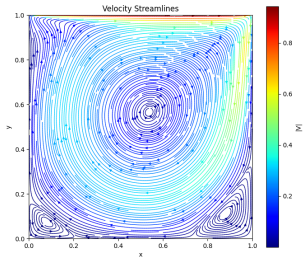

Figure 10: streamlines of velocity magnitude for 257×257 grid, Re=1000

Problem 2: Lid-Driven Cavity with Step

Initial attempts at this problem showed results with velocity streamlines leaking into the solid region and jerky velocities along the boundary walls of the same. This was fixed by better wall boundary condition treatment, which led to no penetration of the walls by the streamlines, a clean pressure field, and smooth convergence of the residuals.

Similar to problem 1, velocity magnitude contours and streamlines were produced, along with pressure contours for the LDC with a step on a 320×320 grid, which are shown in Fig. (11), Fig. (12), & Fig. (13). The masked-out region is clearly seen in these plots, and it should be noted that, similar to the wall boundary conditions from problem 1, all walls, including the walls of the masked-out region, are treated with the no-slip condition. From the streamlines plot, it is clear that the major vortex takes up most of the cavity, similar to that in problem 1, but 3 smaller vortices exist, one at each corner, with the right-hand corner vortex being significantly larger this time around, which can be explained by the higher Reynolds number used for the simulation. It can also be observed that the flow has a tendency to turn along the step corner and stay somewhat adhered instead of forming a larger separation zone. Further, the pressure contour shows a relatively higher pressure zone past the step, caused by the sudden expansion experienced by the flow. It can also be noted from this that, similar to the behavior in the problem 1 pressure plot, the highest pressure is observed in the right-hand lid corner.

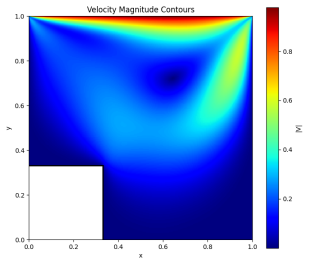

Figure 11: Contour of velocity magnitude for 320×320 grid, Re=200

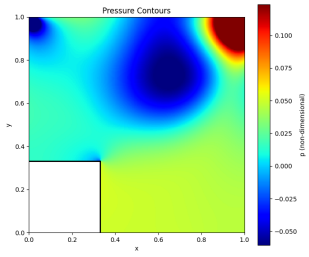

Figure 12: Contour of pressure for 320×320 grid, Re=200

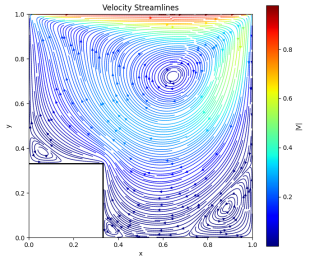

Figure 13: Streamlines of velocity magnitude for 320×320 grid, Re=200

Fig. (14) shows the velocity magnitude contour from the COMSOL simulation of the same domain, which exhibits extremely similar behavior to that of the solver developed. As a further source of validation, the centerline velocities of the solver results were compared to those from the COMSOL solver, as shown in Fig. (15) & Fig. (16), which shows sufficient agreement between the two simulations, validating the results of the solver.

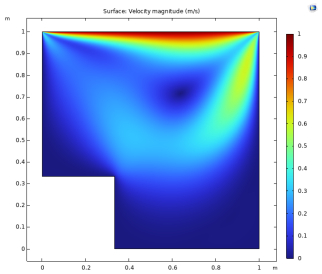

Figure 14: COMSOL validation: Contour of velocity magnitude for 320×320 grid, Re=200

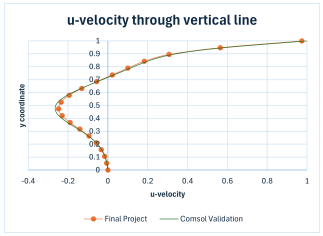

Figure 15: u-velocity through x=0.5

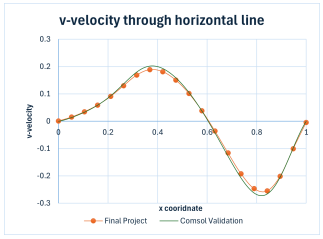

Figure 16: v-velocity through y=0.5

At $Re = 200$, reducing grid size from 129×129 to 320×320 reduces numerical diffusion and truncation error near the step, so the shear layer and recirculation structures are resolved more sharply, the vortex locations stop shifting with grid size, and the pressure field transitions near the internal walls become noticeably steeper and less smeared.

Similar to problem 1, the domain was tested on higher Reynolds numbers by running a 320×320 grid with $Re = 400$ & $Re = 1000$, whose results are in Fig. (17) and Fig. (18), respectively. The streamline plots show that as Re increases, the flow past the step has a tendency to separate earlier. This is consistent with the fact that the lowered viscosity would contribute to a larger separation zone formation in the event of a rapid expansion.

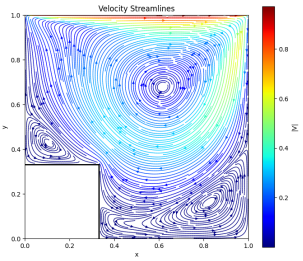

Figure 17: Streamlines of velocity magnitude for 320×320 grid, Re=400

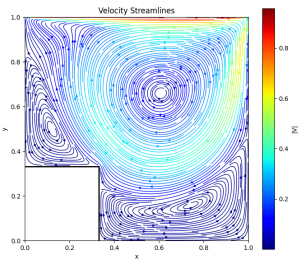

Figure 18: Streamlines of velocity magnitude for 320×320 grid, Re=1000

Additional Domains

Two additional domains were tested to assess the solver's capability of handling changes in L_x & L_y. Fig. (19) shows the streamline plot of a domain with $L_x = 2$ & $L_y = 1$, while $Re = 1000$, while Fig. (20) shows the streamlines of a domain with $L_x = 1$ & $L_y = 2$ with the same Reynolds number.

Both plots show the expected lid-driven behavior, where the highest speeds occur in a thin layer directly under the moving lid, while the interior is dominated by large recirculating vortices, and velocity magnitude decays away from the lid due to viscous effects and wall friction. Both plots also show smaller secondary vortices forming at the corners. It can also be observed that in Fig. (19) the left hand bottom corner vortex is larger than the right hand one, which is the opposite of what is seen in square cavities, whereas in Fig. (20) the circulation breaks up into two side-by-side large vortices separated near the mid-length, with two small corner vortices at the bottom of the cavity.

These figures demonstrate that the lid-driven cavity solution is strongly influenced by geometry/aspect ratio, where when one dimension is doubled, the flow tends to develop multiple primary cells rather than a single dominant vortex

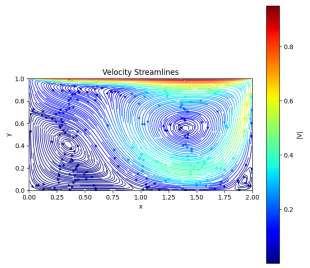

Figure 19: Streamlines of velocity magnitude for $L_x = 2.0$ & $L_y = 1.0$ domain, Re=1000

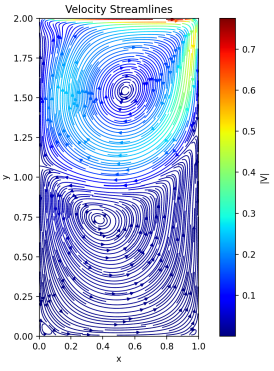

Figure 20: Streamlines of velocity magnitude for $L_x = 1.0$ & $L_y = 2.0$ domain, Re=1000

Conclusion

Overall, this study successfully developed and validated a steady, incompressible Navier–Stokes solver for the lid-driven cavity benchmark using a finite-volume discretization on a collocated grid, coupled through a SIMPLE framework with Rhie–Chow momentum interpolation to ensure stable pressure–velocity coupling and physically consistent face fluxes. The resulting systems were then assembled in sparse form and solved efficiently using GMRES with an AMG preconditioner, allowing the solution to converge to the prescribed continuity tolerance of 10^{-6}.

For problem 1, the flow field that was produced by the solver conformed to the expected physics and was successfully validated by testing the centerline velocities against results from well-accredited literature, as well as a validation simulation developed using the popular commercial package COMSOL Multiphysics. For problem 2, the same methodology was extended to the stepped cavity by treating the step as an internal no-slip wall and enforcing a consistent wall behavior at the internal boundary, producing stable streamlines and pressure fields without leakage into the solid region. The centerline velocities of which were successfully validated against those from the same domain setup in COMSOL Multiphysics. It was also confirmed that the solver is capable of handling a wide range of Reynolds numbers and variations in the physical dimensions of the cavity with numerous test cases.

The convergence study in Appendix (2) confirmed that refinement reduces numerical diffusion and better resolves the shear layer and recirculation near the step, while also ensuring that the results are sufficiently resolved. Any further refinement would result in a higher solver resource requirement for a very slight variation in results.

Apart from mesh size, major contributors to solver runtime and accuracy are under-relaxation factors, GMRES tolerances, and AMG rebuild intervals, and there is a direct accuracy–cost tradeoff in the chosen settings, with a general trend of higher cost giving better accuracy. This trend, however, is not linear, and a safe compromise may be assessed, where adequate accuracy is achieved at acceptable resource costs.

Future Improvements

The present implementation focuses on steady, laminar, 2D flows on uniform Cartesian grids, where accuracy at sharp gradients is limited by the second-order upwind differencing used for convection. A few suggested improvements that could extend the capabilities of the code are as follows:

1. Upgrade convection to higher-order schemes.
2. Add capabilities to run on non-uniform grids or locally refined grids near walls and around the step corner.
3. Add capability of handling other boundary conditions like inlets/outlets.
4. Extend to transient simulation and turbulent flow.
5. Broaden geometry handling by allowing more variation in domain shape and position of step.
6. Extend capability to handle 3D simulations.

References

1. S.V. Patankar and D.B. Spalding. "A Calculation Procedure for Heat, Mass and Momentum Transfer in Three-Dimensional Parabolic Flows". In: *International Journal of Heat and Mass Transfer 15 (1972), pp. 1787–1806.*

2. C.M. Rhie and W.L. Chow. "Numerical Study of the Turbulent Flow Past an Airfoil with Trailing Edge Separation". In: *AIAA Journal 21.11 (1983).*

3. U Ghia, K.N. Ghia, and C.T. Shin. "High-Re Solutions for Incompressible Flow Using the Navier-Stokes Equations and a Multigrid Method". In: *Journal of Computational Physics 48 (1982), pp. 387–411.*

Appendix 1: Numerical Methodology

Non-dimensionalization procedure:

$$x^* = \frac{x}{L} \quad ; \quad y^* = \frac{y}{L}$$
$$u^* = \frac{u}{U} \quad ; \quad v^* = \frac{v}{U}$$
$$P^* = \frac{P}{\rho U^2}$$

$$Here\ x^*, y^*, u^*, v^*, \ \&\ P^{nd}\ are\ non-dimensionalised\ versions\ of\ x, y, u, v, \ \&\ P\ respectively$$

$$Hence\ the\ Eqs.\ become:$$

$$u^* \cdot \nabla^* u^* = \frac{1}{Re}\nabla^{*2} u^* - \nabla^* P^*$$
$$\nabla^* \cdot u^* = 0$$

A] Discretization of the Governing Equations:

$$For\ X-Momentum\ (1):$$

$$\frac{\delta}{\delta x}(\rho uu) + \frac{\delta}{\delta y}(\rho vu) = \frac{\delta}{\delta x}(\mu\frac{\delta u}{\delta x}) + \frac{\delta}{\delta y}(\mu\frac{\delta u}{\delta y}) - \frac{\delta P}{\delta x}$$

$$For\ Y-Momentum\ (2):$$

$$\frac{\delta}{\delta x}(\rho vu) + \frac{\delta}{\delta y}(\rho vv) = \frac{\delta}{\delta x}(\mu\frac{\delta v}{\delta x}) + \frac{\delta}{\delta y}(\mu\frac{\delta v}{\delta y}) - \frac{\delta P}{\delta y}$$

$$For\ Continuity:$$

$$\frac{\delta}{\delta x}(\rho u) + \frac{\delta}{\delta y}(\rho v) = 0$$

$$Integrating\ (1)\ \&\ (2)\ over\ CV$$

$$(\rho uuA)_e - (\rho uuA)_w + (\rho vuA)_n - (\rho vuA)_s = (\mu\frac{du}{dx}A)_e - (\mu\frac{du}{dx}A)_w + (\mu\frac{du}{dy}A)_n - (\mu\frac{du}{dy})_s - (P_eA_e - P_wA_w)$$

$$(\rho uA)_e - (\rho uA)_w + (\rho uA)_n - (\rho uA)_s = 0$$

$$\left.\frac{\delta u}{\delta x}\right|_e = \frac{u_E - u_P}{\delta x_{PE}} \quad ; \quad \left.\frac{\delta u}{\delta x}\right|_w = \frac{u_P - u_W}{\delta x_{WP}} \quad ; \quad \left.\frac{\delta u}{\delta y}\right|_n = \frac{u_N - u_P}{\delta y_{PN}} \quad ; \quad \left.\frac{\delta u}{\delta y}\right|_s = \frac{u_P - u_S}{\delta y_{SP}}$$

$$F = \rho uA \ ; \ D = \frac{\mu A}{\delta x}$$

$$F_eu_e - F_wu_w + F_nu_n - F_su_s = D_e(u_E - u_P) - D_w(u_P - u_W) + D_n(u_N - u_P) - D_s(u_P - u_S) - (P_eA_e - P_wA_w)$$

$$F_e - F_w + F_n - F_s = 0$$

$$Using\ Upwind\ for\ Convection\ \&\ Central\ for\ Diffusion,\ hence:$$

$$a_E = D_e + max(0, -F_e) \quad , \quad a_W = D_w + max(F_w, 0)$$
$$a_N = D_n + max(0, -F_n) \quad , \quad a_S = D_s + max(F_s, 0)$$
$$a_P = a_E + a_W + a_N + a_S + (F_w - F_e + F_s - F_n)$$

$$Hence\ discrete\ momentum\ equations\ are:$$

$$a_P u_P = a_E u_E + a_W u_W + a_N u_N + a_S u_S + (P_w A_w - P_e A_e)$$
$$a_P v_P = a_E v_E + a_W v_W + a_N v_N + a_S v_S + (P_s A_s - P_n A_n)$$

B] Pressure Correction Equation:

$$\frac{\delta \rho}{\delta t} + \frac{\delta(\rho u)}{\delta x} + \frac{\delta(\rho v)}{\delta y} = 0$$

$$\frac{\rho_p - \rho'_p}{\Delta t}\Delta x \Delta y + [(\rho u)_e - (\rho u)_w]\Delta y + [(\rho v)_n - (\rho v)_s]\Delta x = 0$$

$$a_P P'_P = a_E P'_E + a_W P'_W + a_N P'_N + a_S P'_S + S_u$$
$$a_P = a_E + a_W + a_N + a_S$$
$$aE = \rho_e d_e A_e \; ; \; aW = \rho_w d_w A_w \; ; \; aN = \rho_n d_n A_n \; ; \; aS = \rho_s d_s A_s$$
$$d_e = \frac{A_e}{a_e} \; ; \; d_w = \frac{A_w}{a_w} \; ; \; d_n = \frac{A_n}{a_n} \; ; \; d_s = \frac{A_s}{a_s}$$

$$S_u = \frac{\rho'_p - \rho_p}{\Delta t}\Delta x \Delta y + [(\rho u^*)_e - (\rho u^*)_w]\Delta y + [(\rho v^*)_n - (\rho v^*)_s]\Delta x$$

$$For\ Pressure\ \&\ velocity\ correction:$$
$$u = u^* + u' \; ; \; v = v^* + v' \; ; \; P = P^* + P'$$

$$[a_P u_P = \Sigma a_{nb} u_{nb} + (P_w + P_e)A] - [a_P u^*_P = \Sigma a_{nb} u^*_{nb} + (P^*_w + P^*_e)A] = [a_P u'_P = (P'_w + P'_e)A]$$

$$u'_P = \frac{A}{a_P}(P'_w - P'_e)$$

$$\rightarrow \; u = u^* + \frac{A}{a_P}(P'_w - P'_e)$$
$$\rightarrow \; v = v^* + \frac{A}{a_P}(P'_s - P'_n)$$
$$\rightarrow \; P = P^* + P'$$

C] Rhie-Chow Momentum Interpolation method for Pressure-Velocity Coupling:

$$a_e u_e = \Sigma a_{nb} u_{nb} + (S_u - \frac{\delta P}{\delta x})_e V_e$$
$$a_P u_P = \Sigma a_{nb} u_{nb} + (S_u - \frac{\delta P}{\delta x})_P V_P$$
$$a_E u_E = \Sigma a_{nb} u_{nb} + (S_u - \frac{\delta P}{\delta x})_E V_E$$

$$By\ rearranging:$$
$$u_e + \frac{V_e}{a_e}(\frac{\delta P}{\delta x} - S_u)_e = \frac{\Sigma a_{nb} u_{nb}}{a_e}$$
$$u_P + \frac{V_P}{a_P}(\frac{\delta P}{\delta x} - S_u)_P = \frac{\Sigma a_{nb} u_{nb}}{a_P}$$
$$u_E + \frac{V_E}{a_E}(\frac{\delta P}{\delta x} - S_u)_E = \frac{\Sigma a_{nb} u_{nb}}{a_E}$$
$$\frac{\Sigma a_{nb} u_{nb}}{a_e} = \frac{1}{2}[\frac{\Sigma a_{nb} u_{nb}}{a_E} + \frac{\Sigma a_{nb} u_{nb}}{a_P}]$$

$$u_e + \frac{V_e}{a_e}(\frac{\delta x}{\delta x} - S_u)_e = \frac{u_E + u_P}{2} + \frac{1}{2}[\frac{V_e}{a_e}(\frac{\delta P}{\delta x} - S_u) + \frac{V_P}{a_P}(\frac{\delta P}{\delta x} - S_u)_P]$$

$$\rightarrow u_e = \frac{u_E + u_P}{2} + \frac{1}{2}[\frac{V_E}{a_E}(\frac{\delta P}{\delta x} - S_u)_E + \frac{V_P}{a_P}(\frac{\delta P}{\delta x} - S_u)_P] - \frac{V_e}{a_e}(\frac{\delta P}{\delta x} - S_u)_e$$

D] SIMPLE Algorithm implementation procedure:

1. Apply Boundary Conditions
2. Solve x-momentum
3. Solve y-momentum
4. Compute face fluxes using Rhie-Chow interpolation and build continuity residual
5. Solve Pressure-Correction Equation
6. Correct pressure and velocities
7. Repeat until residual < tolerance

Appendix 2: Convergence Study

A mesh convergence study was performed on the Problem 1 domain to ensure that further mesh refinement does not lead to significant changes in the results obtained from the solver and that the solution was adequately resolved.

Two methods of ensuring this were adopted, the first being a qualitative assessment of the u-velocity through x=0.5 and the v-velocity of y=0.5 for the various mesh sizes tested, as shown in Fig. (21(a)) & Fig. (21(b)). It can be observed from both graphs that as grid size increases, the solution becomes more resolved, up until the point where it starts to level and prove consistent despite further refinement. This is evidently observed between the 129×129 and 257×257 plots, where both curves are of the same shape to a considerable margin.

Secondly, a qualitative test was performed using the u_{min} along the x=0.5 line upto a threshold of 1.5% relative percentage change. The primary recirculation induces a strong negative u along x=0.5, where the most negative value traces the strength of the primary vortex. This metric is simple but acceptable in our case, as it is a further step taken to ensure the observations from the qualitative tests were accurate. The results of this test show that the relative % change is 1.16%, which is under the threshold, when grid size changes from 129×129 and 257×257, leading to a positive grid convergence result.

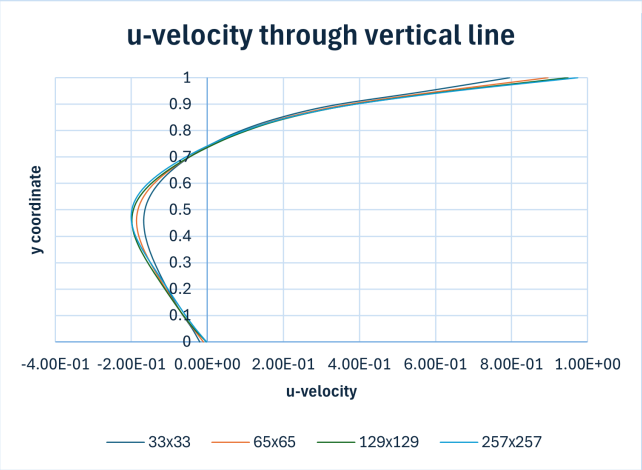

(a) u-velocity through x=0.5 for different mesh sizes

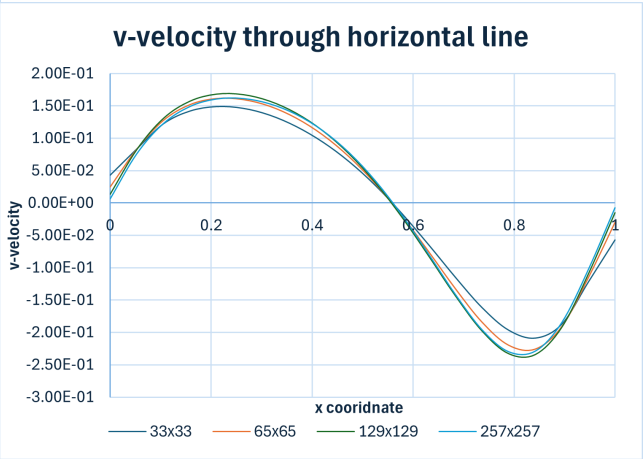

(b) v-velocity through y=0.5 for different mesh sizes

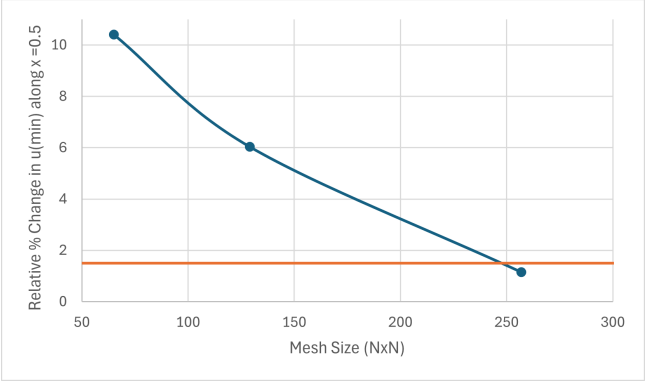

(c) Relative % change in u_{min} along x=0.5

Figure 21: Convergence Study Graphs